

# Simultaneous measurements of nuclear spin heat capacity, temperature and relaxation in GaAs microstructures.

M. Vladimirova, S. Cronenberger, A. Colombier, D. Scalbert  
*Laboratoire Charles Coulomb, UMR 5221 CNRS/Université de Montpellier, France*

V. M. Litvyak, K. V. Kavokin  
*Spin Optics Laboratory, St. Petersburg State University, Ulyanovskaya 1, St. Petersburg 198504, Russia*

A. Lemaître  
*Université Paris-Saclay, CNRS, Centre de Nanosciences et de nanotechnologies, 91120, Palaiseau, France*  
 (Dated: December 7, 2021)

Heat capacity of the nuclear spin system (NSS) in GaAs-based microstructures has been shown to be much greater than expected from dipolar coupling between nuclei, thus limiting the efficiency of NSS cooling by adiabatic demagnetization. It was suggested that quadrupole interaction induced by some small residual strain could provide this additional reservoir for the heat storage. We check and validate this hypothesis by combining nuclear spin relaxation measurements with adiabatic remagnetization and nuclear magnetic resonance experiments, using electron spin noise spectroscopy as a unique tool for detection of nuclear magnetization. Our results confirm and quantify the role of the quadrupole splitting in the heat storage within NSS and provide additional insight into fundamental, but still actively debated relation between a mechanical strain and the resulting electric field gradients in GaAs.

## I. INTRODUCTION

In n-doped semiconductors two spin ensembles, donor-bound electron spins and the lattice nuclei spin system (NSS) are coupled via hyperfine interaction [1]. Their magnetic moments, interaction energies, their coupling to light, to crystal lattice vibrations, as well as to electric and magnetic fields differ dramatically. The resulting physics, that is best studied in n-GaAs, is quite complex. However, if sufficient NSS stability is reached, it may potentially offer novel applications for quantum information technologies [2–10].

In this context, precise knowledge and control of nuclear quadrupole effects in n-GaAs and GaAs-based heterostructures has attracted substantial attention. Indeed, in semiconductors with cubic symmetry containing isotopes with spin  $I > 1/2$  quadrupole interaction induced by strain splits NSS energy states (*cf* Fig. 1 (b)) and thus strongly affects NSS thermodynamics [11–14]. Nevertheless the quantitative results remain controversial [15–18]. This is partly due to the lack of non-destructive and non-perturbative experimental techniques, capable of probing NSS at low and zero magnetic field, where quadrupole splittings between spin levels dominate over Zeeman ones.

Electron spin noise spectroscopy (SNS) could be promising for this purpose. Indeed, it has been shown that SNS can non-destructively relay properties of nuclear environment through the statistics of electron spin interaction with the total nuclear polarization, see Fig. 1 (c-d) [19–22]. SNS is based on the non-perturbative detection of the electron magnetization noise via fluctuations of the Kerr or Faraday rotation of the off-resonant laser beam polarization [23, 24]. In

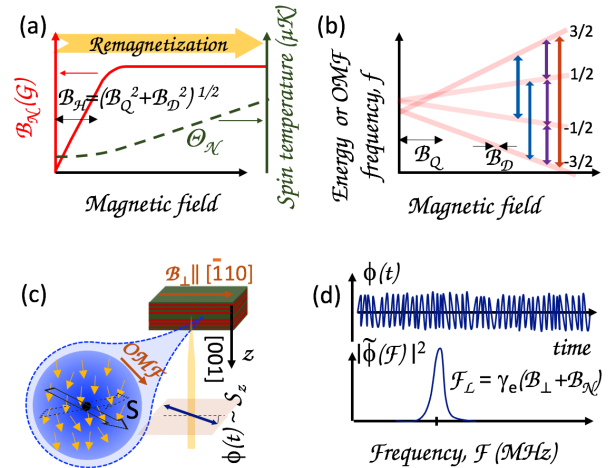


Figure 1. (a) Overhauser field  $B_N$  and the corresponding nuclear spin temperature  $\Theta_N$  as a function of the magnetic field according to spin temperature theory.  $B_H$  is a field that characterizes NSS heat capacity. (b) Schematic representation of quadrupole-split nuclear spin levels. Arrows indicate NMR transitions (c) Sketch of the donor-bound electron spin interacting with the underlying nuclear spins. (d) Fluctuations of the electron spin detected via Faraday rotation in time domain within 0.5 GHz frequency band and the corresponding Fourier power spectrum.

order to increase sensitivity the homodyne detection scheme has been implemented [25–27].

Any variation of the NSS polarization results in a shift of the electron spin noise frequency peak proportional to the Overhauser field  $B_N$ , an effective nuclear field resulting from the hyperfine interaction (Fig. 1 (d)). A particularly high SNS sensitivity could be reached in n-

GaAs layers embedded in a microcavity, allowing us to monitor with sub-second resolution (i) NSS relaxation under an arbitrary magnetic field [28] and (ii) NSS re-magnetization through zero field, where its physics is ruled by the spin temperature theory [29].

These experiments revealed a dramatic enhancement of the NSS warm up rates in n-GaAs under magnetic fields below 10 G, and a huge heat capacity characterized by so-called local field, also of order of  $\approx 10$  G. This value is much higher than expected from magnetic dipole-dipole interaction  $B_D \approx 1.5$  G [30]. This is illustrated in Fig. 1 (a). It shows variation of the nuclear spin temperature (dashed line) and Overhauser field (solid line) in a cold NSS during re-magnetization from zero to high magnetic field. The magnetic field below which  $\Theta_N$  remains constant reveals enhanced heat capacity of the NSS. In the following it will be referred to as heat capacity field,  $B_H$  [31]. Because in GaAs the spin of all isotopes  $I = 3/2$ , it was suggested that such enhanced NSS heat capacity could be explained by the quadrupole splitting of nuclear spin energy levels induced by some small residual strain, see Fig. 1 (b). The corresponding effective field  $B_Q$  is the one where Zeeman and quadrupole energies become comparable. In re-magnetization experiment illustrated in Fig. 1 (a) one would expect

$$B_H = \sqrt{B_D^2 + B_Q^2}. \quad (1)$$

In this work we implement a new technique, nuclear magnetic resonance (NMR) detected by electron SNS, in order to verify this hypothesis. NSS absorption spectra in the radio-frequency (RF) range are measured as a function of magnetic field from zero to 100 G. The analysis of these spectra allows us to (i) evaluate quantitatively quadrupole energies and confirm the impact of the quadrupole interaction on the heat capacity of the NSS. The quadrupole energies extracted from the NMR spectra appear to be consistent with heat capacity fields measured in the NSS re-magnetization experiments and with the spin temperature theory; (ii) to provide additional insight into relative values of so-called gradient-elastic tensor  $S_{ijkl}$  for Ga and As isotopes. This fundamental parameter determines the relation between the strain tensor  $\epsilon_{kl}$  and the resulting gradients of electric fields at each atomic site  $V_{ij} = \sum_{k,l} S_{ijkl} \epsilon_{kl}$ . Its values are isotope-dependent and are still actively debated in the literature [15–18].

## II. SAMPLE

We study the microcavity sample cut out from the same wafer as in Ref. 29: a Si-doped  $3\lambda/2$  GaAs layer (cavity mode at  $\approx 830$  nm in the studied piece of the sample) with donor concentration  $n_D \approx 2 \times 10^{15} \text{ cm}^{-3}$  sandwiched between two Bragg mirrors, in order to enhance the sensitivity of the SNS (quality factor  $\approx 2 \times 10^4$ ).

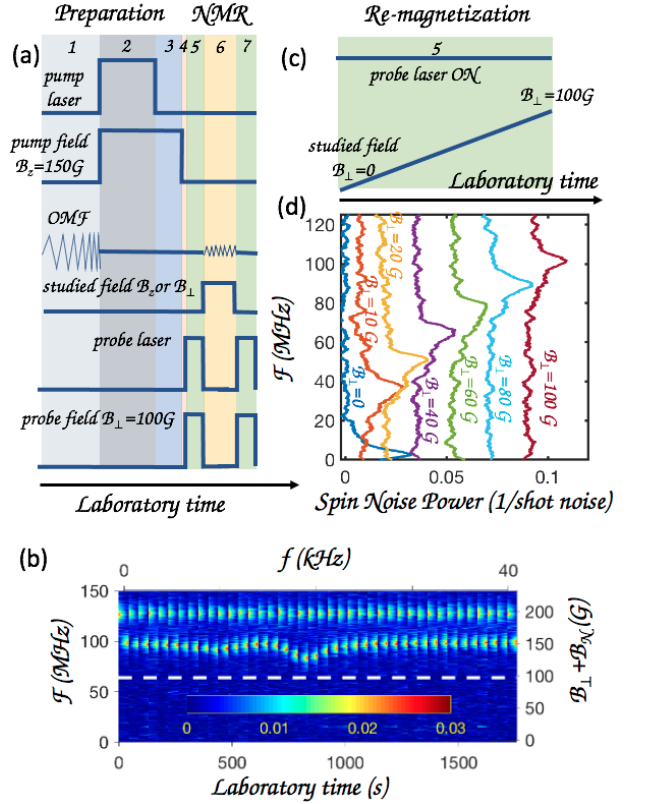


Figure 2. Time-sequence used in NMR (a) and re-magnetization (c) experiments. Preparation sequence in (c) is identical to (a), not shown. (b) An example of 40 pairs of color-encoded SN spectra, each pair recorded within the time-sequence (a) for different OMF frequencies, that allow us to reconstruct the RMN spectrum at  $B = 0$ . (d) Typical SN spectra measured at different magnetic fields during adiabatic re-magnetization.

The front (back) mirrors are distributed Bragg reflectors composed of 25 (30) pairs of AlAs/Al<sub>0.1</sub>Ga<sub>0.9</sub>As layers. The sample is grown on a 400- $\mu\text{m}$ -thick [001]-oriented GaAs substrate and placed in a cold finger cryostat at  $T=6$  K. A 30-spire copper coil is placed on top of the sample to create an oscillating magnetic field (OMF). It is directed at  $45^\circ$  out of the sample plane [32].

## III. NMR AND RE-MAGNETIZATION DETECTED BY THE ELECTRON SPIN NOISE

The principle of NMR and NSS re-magnetization detected by electron spin noise are sketched in Fig. 2 (a) and (c), respectively. Prior to the measurement, any preexisting polarization in the NSS is erased by OMF  $B_{RF} = 0.3$  G during 20 s, its frequency sweeping between 0 and 50 kHz (stage 1). At second stage the NSS is polarized by optical pumping in the presence of a longitudinal magnetic field  $B_z = 150$  G during typically 30s (circularly polarized laser diode emitting at 770 nm).

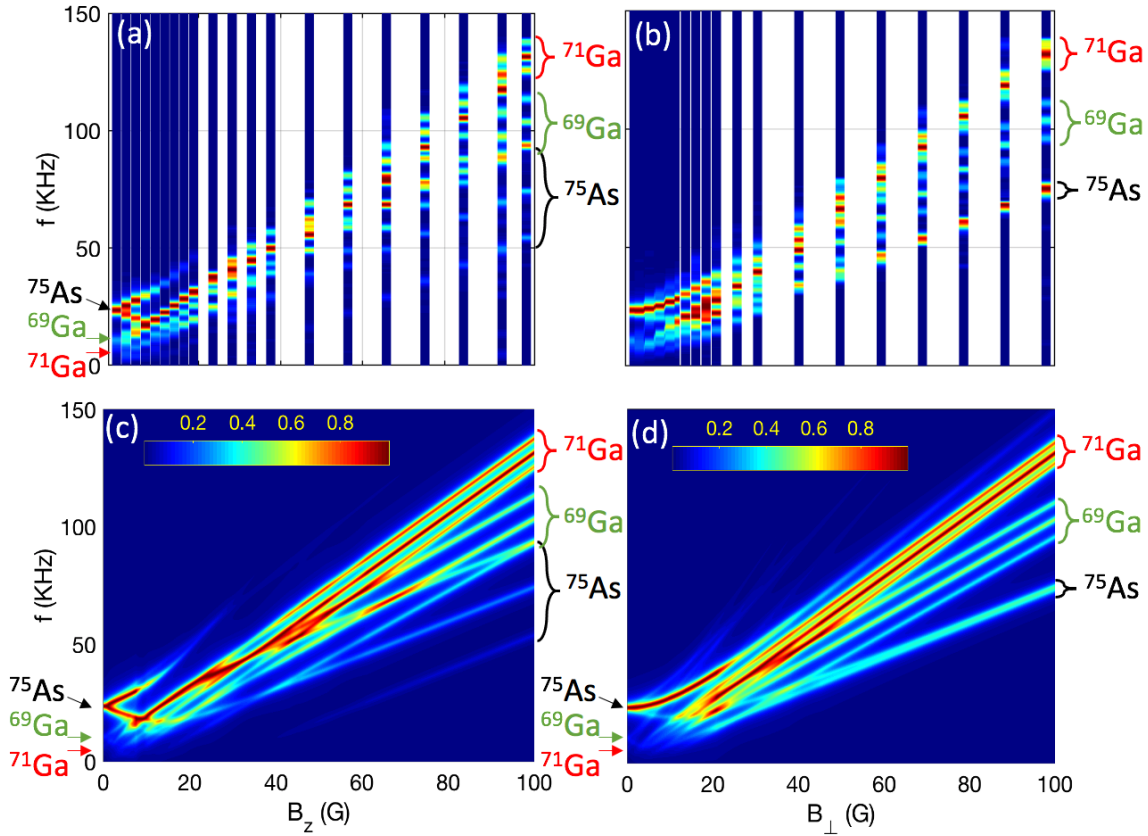


Figure 3. Color-encoded NSS absorption spectra measured (a, b) and calculated (c, d) at different values of magnetic field parallel to either  $[110]$  (b) or  $[001]$  (a) crystallographic axis. All the spectra are normalized to unity.

This is followed by 30 s of dark time under the same magnetic field to allow for fast relaxation of the nuclear spins under the donors orbits while keeping bulk nuclei polarized (stage 3) and then adiabatic demagnetization down to zero magnetic field (stage 4). This last stage ensures the thermalization of the NSS and a transfer of the optically pumped energy stored in Zeeman reservoir towards internal degrees of freedoms, that is dipole-dipole reservoir. The four stages preparation of the NSS is identical for both NMR and re-magnetization experiments.

The re-magnetization experiments are similar to those reported in Ref. 29. After preparation stages 1–4, a set of electron spin noise spectra under in-plane magnetic field that increases from  $B = 0$  to  $B = 100$  G is measured every 2 G, see Fig.2 (c). The measured frequency  $F_L$  of the electron spin noise spectral peak at a given field  $B_{\perp}$  is directly related to the Overhauser field  $B_N$ ,

$$F_L = F_B + F_N = \gamma_e(B_{\perp} + B_N), \quad (2)$$

where  $\gamma_e = 0.62$  MHz/G is the electron gyromagnetic ratio in GaAs. Representative spectra measured at several values of magnetic field are shown in Fig.2 (d).

Measurement of each point of the NMR spectrum consists in three steps: detection of electron spin noise

in the sample under magnetic field  $B_{\perp} = 100$  G in order to evaluate the Overhauser field prior to absorption (stage 5), application during 3 s of the oscillating magnetic field at a given frequency  $f$  in the RF range and at a given magnetic field at which the RF absorption needs to be addressed (stage 6), and again detection of electron spin noise spectrum under magnetic field  $B_{\perp} = 100$  G, to measure to which extent the Overhauser field has decreased (stage 7).

The shift between the electron spin noise spectral peaks measured during stages 5 and 7 contains two contributions. The first is RF-independent, it is due to weak, but unavoidable NSS relaxation during measurement. It can be evaluated for by performing identical measurements without RF field in stage 6. The second contribution is proportional to the NSS absorption at a given OMF frequency  $f$ . When  $f$  matches the energy difference between spin states of one of the isotopes the radiation is efficiently absorbed. The entire absorption spectrum (or NMR spectrum) can be constructed by repeating the protocol (stages 1-7) at different values of  $f$ . The details of this procedure are given in Appendix X A.

An example of the raw data obtained in a NMR experiment addressing NSS absorption at  $B = 0$  is shown in Fig. 2 (b). Color-encoded series of electron spin noise spectra measured in the units of the ratio between spin

and shot noise are shown as a function of both laboratory time (lower scale) and OMF frequency  $f$  (upper scale). For each value of  $f$  two spectra are systematically measured, one before application of the OMF (in this case the electron spin noise peak frequency  $F_L$  does not depend on the OMF frequency  $f$ ), and one after. Left scale shows spin noise frequency and right scale corresponding total magnetic field experienced by the electrons,  $B_{\perp} + B_N$ , where  $B_{\perp} = 100$  G. One can see that  $B_N$  is significantly smaller after application of the OMF at  $f \approx 8$  kHz and at  $f \approx 20$  kHz. These frequencies characterize nuclear spin splittings at  $B = 0$ , cf Fig. 1 (a). We anticipate, that the higher frequency is related to quadrupole-split states of  $^{75}\text{As}$  which has the highest quadrupole moment, and the lower one to closely lying transitions of  $^{71}\text{Ga}$  and  $^{69}\text{Ga}$  isotopes.

It is important to note that in most of SNS experiments the magnetic field is modulated to eliminate spin-independent signals [33]. Such approach is not suitable for studies of the NSS, because nuclear spins get depolarized by non-adiabatically varying magnetic fields. To avoid this effect and also increase the sensitivity, in this work we use a homodyne detection scheme [25]. This allows us to use the probe power as low as  $150 \mu\text{W}$  focused on  $30 \mu\text{m}$ -diameter spot. We detect the spectra in two mutually orthogonal linear polarizations, that is either parallel (which contains useful information about electron spin noise) or orthogonal to the local oscillator polarization. The spin noise spectrum is obtained by taking the difference between these spectra, in order to get rid of the background noise.

#### IV. NMR SPECTRA AND THEIR INTERPRETATION

A set of color-encoded NMR spectra measured under in-plane static magnetic field  $B_{\perp} \parallel [110]$  and at  $B_z \parallel [001]$ , is shown in Fig. 3 (a-b). In order to understand these spectra in terms of the OMF-induced transitions between spin states of the three GaAs isotopes, we must calculate the energy spectrum of the NSS. It is determined by quadrupole interaction and Zeeman effects:  $\hat{H}^i = \hat{H}_Q^i + \hat{H}_Z^i$ , where  $\hat{H}_Q^i$  ( $\hat{H}_Z^i$ ) describes quadrupole (Zeeman) interaction [34]. The energy levels of each isotope are given by the eigenvalues of the hamiltonian  $\hat{H}^i$ , and the NMR transitions frequencies by their differences  $f_{kl}^i = (E_k^i - E_l^i)/h$ , where  $h$  is the Plank constant. The OMF induces spin transitions between a pair of states  $k$  and  $l$  of  $i$ -th isotope, if the OMF frequency matches the energy difference between their energy levels  $E_k$  and  $E_l$ . The probability of corresponding transition is given by  $P_{kl}^i \propto M_{kl,i}^2$ , where  $M_{kl} = \langle \Psi_k | H_{OMF} | \Psi_l \rangle$  is the matrix element of the Hamiltonian describing Zeeman interaction of the nuclear spins with the OMF.

The quadrupole Hamiltonian of the  $i$ -th isotope in the presence of the in-plane biaxial strain can be written as

[11]:

$$\hat{H}_Q^i = \frac{E_{QZ}^i}{2} \left[ \hat{I}_z^2 - \frac{I(I+1)}{3} \right] + \frac{E_{QR}^i}{2\sqrt{3}} \left[ (\hat{I}_x^2 - \hat{I}_y^2) \right] + \frac{E_{QI}^i}{2\sqrt{3}} \left[ (\hat{I}_x \hat{I}_y + \hat{I}_y \hat{I}_x) \right], \quad (3)$$

where  $E_{QR}^i = E_{Q\perp}^i \cos 2\zeta^i$  and  $E_{QI}^i = E_{Q\perp}^i \sin 2\zeta^i$ . It is determined by three parameters:  $E_{QZ}^i$  - the quadrupole energy along growth axis,  $E_{Q\perp}^i$  - the in-plane quadrupole energy, and  $\zeta^i$  - the angle between the principal axis of the electric field gradient tensor  $V_{ij}$  and the [100] crystal axis.

The ensemble of the absorption spectra shown in Fig. 3 (a-b) can be understood by fitting this simple model to the observed transition frequencies. This yields 3 parameters per isotope. They are summarized in Table I together with other relevant parameters (abundances, quadrupole moments and gyromagnetic ratios) taken from the literature. Assuming that all transitions have Lorentzian shape broadened by dipole-dipole interaction ( $\Delta f_D = 1.5$  kHz), we calculate the resulting absorption spectra at different values and two orientations of the magnetic field as shown in Fig. 3 (c-d).

One can see that most of salient features of the measured spectra are faithfully reproduced. At  $B = 0$  the  $^{75}\text{As}$  absorption (higher frequency line) dominates the spectrum. At small fields parallel to the growth axis  $B_z$  the  $^{75}\text{As}$  absorption line splits into two lines, that shift linearly with  $B_z$ . By contrast, under in-plane field  $B_{\perp}$  the  $^{75}\text{As}$  absorption line shifts quadratically. At strong field  $B = 100$  G we identify for each isotope a triplet of lines, including a central line and a pair of satellites. The strongest absorption is observed for  $^{71}\text{Ga}$ . In the presence of the longitudinal field  $B_z$  the splitting between central line and its satellites is the smallest for  $^{71}\text{Ga}$  and the highest for  $^{75}\text{As}$ . By contrast, under an in-plane field  $B_{\perp}$  this splitting vanishes for  $^{75}\text{As}$ . This later fact results from the sign difference in the in- ( $E_{QI}$ ) and out-of-plane ( $E_{QZ}$ ) quadrupole parameters for Ga and As. We will show below that this implies a particular sign relation between different elements of the gradient-elastic tensor elements  $S_{11}$ ,  $S_{44}$  for Ga and As.

#### V. RE-MAGNETIZATION OF THE NSS IN THE PRESENCE OF THE QUADRUPOLE EFFECTS

The above measurements show that quadrupole interaction is much stronger in this sample than dipole-dipole interaction. In this section we compare quantitatively the quadrupole splittings and effective field  $B_Q$  that they should induce with the actual heat capacity field  $B_H$  characterizing NSS re-magnetization.

The spin temperature theory states that in a NSS isolated from the lattice an equilibrium state characterized

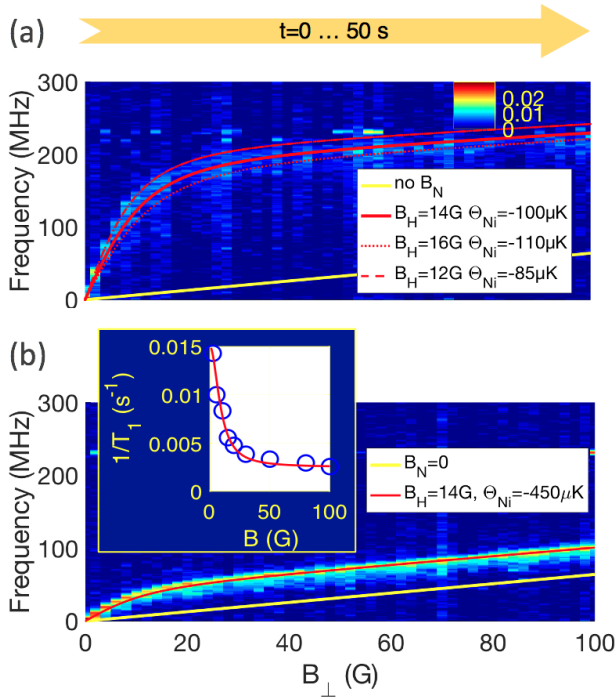


Figure 4. Color-encoded SN spectra (in signal to shot noise ratio units) during the adiabatic demagnetization procedure preceded by preparation of nuclei including either 4 minutes (a) or 30 s optical pumping (b). Red lines are fit to spin temperature model assuming  $B_H = 14 \pm 2$  G and taking into account spin relaxation. Yellow line shows the external field contribution to the spin noise frequency,  $F_N$ . Inset shows the inverse nuclear spin relaxation time as a function of the magnetic field (symbols) measured under the pumping conditions of (b). Solid line is a Lorentzian fit to the data used to calculate red lines.

by the temperature  $\Theta_N$  will be established within a characteristic time  $T_2 \approx h/\gamma_N B_D$  [35]. On time scales larger than  $T_2$  and shorter than  $T_1$ , and provided that  $T_2 \ll T_1$ , where  $T_1$  is spin-lattice relaxation time, the NSS can be considered as isolated from the lattice. If NSS is prepared at temperature  $\Theta_{Ni}$  under magnetic field  $B_i$  and subjected to a slowly varying magnetic field, such that  $dB/dt < B_D/T_2$ , then  $\Theta_N$  and the Overhauser field  $B_N$  change obeying universal expressions [29, 35–37]:

$$B_N = \frac{hBb_N I(I+1) \sum_i A_i \gamma_{Ni}}{3k_B \Theta_N}; \quad \frac{\Theta_N}{(B^2 + B_H^2)^{1/2}} = \frac{\Theta_{Ni}}{B_i}. \quad (4)$$

Here  $A_i$  ( $\gamma_{Ni}$ ) is the abundance (gyromagnetic ratio) of  $i$ -th isotope (see Table I),  $k_B$  is the Boltzmann constant,  $b_N$  is the Overhauser field at saturation of the nuclear magnetization, in GaAs  $b_N = 5.3$  T.

It was assumed for many years that the heat storage in bulk semiconductor NSS is dominated by dipole-dipole interaction. Our recent measurements of the Overhauser field in the presence of the slowly varying external magnetic field overturned this assumption and pointed out possible contribution of strain-induced

quadrupole interaction, see Eq. (1) [29]. The effective field due to quadrupole interaction can be calculated as [20]:

$$B_Q = \frac{4 \sum_i A_i (E_{Q\perp}^2 + E_{QZ}^2)}{5 \sum_i A_i \gamma_{Ni}^2}. \quad (5)$$

This yields  $B_Q^{NMR} = 16$  G using the quadrupole energies extracted from the NMR spectra. This value needs to be compared with  $B_H$  from Eq. (4) that fits the re-magnetization experiments.

Figure 4 shows two sets of the spin noise spectra measured in a re-magnetization experiment starting from  $B_i = 0$  for two different initial nuclear spin temperatures obtained by optical pumping during 4 minutes (a) and 30 s (b). The peak in the electron spin noise spectrum shifts from zero at  $B = 0$  to  $\approx 230$  MHz ( $\approx 100$  MHz) at  $B_\perp = 100$  G in the NSS cooled during 120 (30) seconds. Longer optical cooling yields lower NSS temperatures and higher Overhauser field reached in the former case, while the contribution to the external field is identical in these two experiments. It is shown by the yellow line. One can see that the rapid growth of the frequency at small fields is followed by much slower growth at higher fields. The latter is essentially due to the external field. In the framework of the spin temperature theory, the characteristic magnetic field where the slope changes is of the order of heat capacity field  $B_H$ . Red lines calculated using Eqs. (1),(2), (4 with  $B_i = 0$ ), assuming  $B_H = 14 \pm 2$  G and  $\Theta_{Ni}$  as a fitting parameter are shown in Fig. 4 on top of the color-encoded spin-noise spectra. The magnetic field dependent NSS relaxation on the time scale of the measurement (50 s) is taken into account in this calculation. The corresponding values of  $1/T_1$  measured in a separate set of experiments are shown in the inset. One can see that within the experimental accuracy which is mainly given by the unavoidable warm-up of the NSS during measurements  $B_H \approx B_Q = 14 \pm 2$  G matches quite well the value  $B_Q^{NMR} = 16$  G.

Importantly, NMR and re-magnetization measurements were done at very close points on the sample surface. Indeed, it has been shown that the strain varies in the plane of GaAs substrates, epilayers, quantum wells and microstructures [18, 40–44]. A different set of NMR experiments performed at another point yielded a smaller value of  $B_Q^{NMR} = 12$  G, correlated with smaller  $B_Q = 9 \pm 2$  G extracted from the corresponding re-magnetization experiments.

Note that the NSS relaxation enhancement at small fields has also been attributed to the presence of quadrupole effects in the similar samples [28, 45]. This so-called quadrupole relaxation is induced by fluctuating donor charges, and the resulting enhancement of the relaxation rate as compared to the strong field relaxation rate  $1/T_\infty$  is given by the same heat capacity field

	<sup>69</sup> Ga	<sup>71</sup> Ga	<sup>75</sup> As	<sup>75</sup> As/Ga
Q (10 <sup>-30</sup> m <sup>2</sup> ) [38]	10.7	17.1	31.4	
Abundance	0.3	0.2	0.5	
γ <sub>N</sub> (kHz/G) [38]	0.82	0.64	0.45	
C <sub>11</sub> (10 <sup>-10</sup> N/m <sup>2</sup> ) [39]	12	12	12	
C <sub>12</sub> (10 <sup>-10</sup> N/m <sup>2</sup> ) [39]	5.4	5.4	5.4	
C <sub>44</sub> (10 <sup>-10</sup> N/m <sup>2</sup> ) [39]	6.2	6.2	6.2	
E <sub>QZ</sub> /h (kHz)	-10±0.5	-6±0.5	20±0.5	
E <sub>⊥</sub> /h (kHz)	-3.5±0.5	-2.2±0.5	12.5±0.5	
ζ (degrees with [100] axis)	-68±5	-68±5	-33±5	
S <sub>11</sub> (10 <sup>21</sup> V/m <sup>2</sup> )	-31.7[15], -22 [16]	-31.7[15], -22 [16]	34[15], 24.2 [16]	-1.07 [15], -1.1 [16, 18]
S <sub>11</sub> (10 <sup>21</sup> V/m <sup>2</sup> ) [this work]				<b>-1.1±0.1</b>
S <sub>44</sub> (10 <sup>21</sup> V/m <sup>2</sup> )	32[15], 9[17]	32[15], 9[17]	68[15], 48[17]	2.1[15], 5.3[17], 1.9 [18]
S <sub>44</sub> (10 <sup>21</sup> V/m <sup>2</sup> ) [this work]				<b>2.5±0.4</b>

Table I. Quadrupole parameters obtained in this work and those taken from the literature, as well as other GaAs parameters used in the calculations: stiffness tensor elements, isotope abundancies, quadrupole moments and gyromagnetic ratios.

$B_H$ , see Eq. (1):

$$\frac{1}{T_1} = \frac{1}{T_\infty} + \frac{1}{T_Q}; \quad \frac{1}{T_Q} \propto 1/(B^2 + B_H^2). \quad (6)$$

Fitting the experimental values of the NSS relaxation rate (Fig. 4, inset) to the Eq. (6) returns the value  $B_Q^r = 9$  G which is slightly smaller, but still close to the values returned by NMR and re-magnetization experiments. These results strongly support the ideas put forward in Refs. 28, 29, and 45. Namely, the electric field gradients in the NSS containing isotopes with the spin  $I > 1/2$  lead to quadrupole effects which are detrimental to both nuclear spin memory and adiabatic demagnetization efficiency.

## VI. ESTIMATION OF GRADIENT-ELASTIC TENSOR ELEMENTS

In this section we further analyze the quadrupole parameters determined from NMR experiments and extract relevant information on the stress intensity and orientation, as well as on the elements of the gradient-elastic tensor  $S_{ijkl}$  - an important material parameter relating electric field gradients on the atomic sites with the strain experienced by the crystal. In the crystals with cubic symmetry like GaAs, it can be reduced to two components,  $S_{11}$  and  $S_{44}$ . The interest in this tensor has emerged recently, both in view of non-destructive characterization of the strain, and in the context of exploration of coherent electron-nuclei spin dynamics in GaAs quantum dots.

The three isotope-dependent parameters that we extract from the NMR spectra are related to the three isotope-independent parameters which characterize the in-plane biaxial stress experienced by the crystal: values of the pressure applied in two orthogonal directions ( $p_1$ ,  $p_2$ ) and the angle  $\zeta$  between the stress principal axis and

[100] crystallographic axis. Their derivation is given in Section X B [46]:

$$E_{QZ}^i = -\frac{3eQ^i S_{11}^i}{4I(2I-1)} \frac{p_1 + p_2}{C_{11} - C_{12}}, \quad (7)$$

$$E_{Q\perp}^i \cos 2\zeta^i = \frac{3\sqrt{3}eQ^i S_{11}^i}{4I(2I-1)} \frac{p_1 - p_2}{C_{11} - C_{12}} \cos(2\zeta), \quad (8)$$

$$E_{Q\perp}^i \sin 2\zeta^i = \frac{\sqrt{3}eQ^i S_{44}^i}{2I(2I-1)} \frac{p_1 - p_2}{C_{44}} \sin(2\zeta). \quad (9)$$

Here  $e$  is the absolute value of the electron charge,  $C_{11}$ ,  $C_{12}$  and  $C_{44}$  are known stiffness tensor components,  $E_{QZ}^i$ ,  $E_{Q\perp}^i$  and  $\zeta^i$  are the parameters of the Hamiltonian 3 determined from the fit to the NMR spectra. Their values are given in Table I.

Eqs. (7)-(9) are not sufficient to fully characterize five independent parameters ( $p_1$ ,  $p_2$ ,  $\zeta$ ,  $S_{11}^i$ ,  $S_{44}^i$ ) for each isotope. However, they allow us to ascertain the ratio between the values of gradient elastic tensor components  $S_{11}^{69\text{Ga}}/S_{11}^{75\text{As}}$  and  $S_{44}^{69\text{Ga}}/S_{44}^{75\text{As}}$ . Since both Ga isotopes experience the same electrostatic environment, these ratios are expected to be identical for <sup>71</sup>Ga. This appears to be the case within our experimental precision. In the following we denote both isotopes as Ga, to simplify the notations.

The obtained values of the gradient elastic tensor elements are summarized in Table I, and compared with previous results. The component  $S_{11}$  of the gradient-elastic tensor contributes to both in and out-of-plane quadrupole energies, see Eqs 7-8. In particular, it is proportional to  $E_{QZ}$ , that dominates over in-plane quadrupole splitting  $E_{Q\perp}$  in our sample. One can see that  $S_{11}^{\text{Ga}}/S_{11}^{75\text{As}} = -1.1 \pm 0.1$  matches quite well the conclusions of Refs. 15, 16, and 18, corroborating their results.

However for  $S_{44}^{\text{Ga}}/S_{44}^{75\text{As}}$  the discrepancy between the existing values is very substantial. Our value  $2.5 \pm 0.4$  is rather close to that of Refs. 15 and 18, and much smaller than the result of Ref. 17. At this stage we don't have any explanation for these discrepancies, but such a strong dispersion of  $S_{44}$  measured in different experiments suggests that further studies are mandatory to resolve this issue.

## VII. EVALUATION OF THE BUILT-IN STRESS AND DISORDER

In order to estimate the stress parameters  $p_1$ ,  $p_2$  and  $\zeta$  Eqs. (7)-(9) are not sufficient and we need to use the values of  $S_{11}$  measured elsewhere. We rely on recent values of Chekhovich et al [16], [47]. For the point where the complete set of NMR spectra has been measured (see Fig. 3) this yields  $p_1 + p_2 = 29.5$  MPa,  $p_1 - p_2 = 14$  MPa,  $\zeta = 55^\circ$  degrees, bearing in mind that relative sign of  $p_1 + p_2$ ,  $p_1 - p_2$  and  $\zeta$  is not uniquely defined. Measurements performed in other points of the sample revealed variation of the quadrupole energies up to 30%. This is consistent with the disorder effects reported in GaAs microcavities [42–44], as well as in bulk GaAs samples [18, 40].

## VIII. CONCLUSIONS

In this work we develop and implement a new technique that allows us to probe NMR by electron spin noise spectroscopy. These experiments aim to quantify quadrupole effects in the NSS of n-GaAs. The NSS absorption spectra in a n-GaAs epilayer embedded in a microcavity are measured under magnetic field in the range from zero to 100 G, either parallel or perpendicular to the growth axis. The ensemble of the spectra determines unambiguously the parameters of the quadrupole Hamiltonian, and thus relevant splittings between nuclear spin states for each of three GaAs isotopes. These measurements are particularly relevant at zero and weak magnetic fields, because the spin states splittings are dominated by quadrupole interaction rather than by Zeeman effect, and only few experimental methods give access to zero- and low-field NMR [18, 48].

Our results establish a connection between the residual strain giving rise to quadrupole splittings, the increased heat capacity and nuclear spin relaxation rates at low and zero field. Indeed, from the quadrupole parameters measured by NMR we estimate that heat capacity field limiting NSS cooling by adiabatic demagnetization and increasing NSS spin relaxation rate is of order of  $B_Q^{\text{NMR}} = 16 \pm 2$  G. This value is close to  $B_Q = 14 \pm 2$  G measured at very close point on the sample surface in a set of separate adiabatic demagnetization experiments using SNS as a detection tool. More

precise measurements are complicated due to variation up to 30% of the quadrupole energies and thus nuclear warm up rates induced by inhomogeneity of the local strain on the scale of several millimeters across the sample surface. Nevertheless our results strongly support the model of quadrupole-limited NSS cooling [29] and quadrupole-driven NSS warm up [28, 45].

From the quadrupole hamiltonian we also obtain an estimation of the gradient-elastic tensor that relates gradients of the electrostatic potential on each nuclear site with the strain tensor. Since we don't have an independent measurement of the stress present in the sample, we are limited to the determination of only relative values of the two relevant gradient-elastic tensor elements for different isotopes,  $S_{11}$  and  $S_{44}$ . It appears that  $S_{11}^{\text{Ga}}/S_{11}^{75\text{As}} = -1.1 \pm 0.1$  matches quite well the conclusions of Refs. 15, 16, and 18, while for  $S_{44}^{\text{Ga}}/S_{44}^{75\text{As}}$ , where a big discrepancy exist between the values in the literature, we get  $S_{44}^{\text{Ga}}/S_{44}^{75\text{As}} = 2.5 \pm 0.4$ , rather close to that of Refs. 15 and 18, and much smaller than the result of Ref. 17. Understanding of discrepancies in the  $S_{44}$  values involved in the presence of an in-plane shear strain calls for further studies.

## IX. ACKNOWLEDGEMENTS

The authors are grateful to R. Cherbunin and V. K. Kalevich for enlightening discussions, and acknowledge financial support from Russian-French grant CONUS (Russian Foundation for Basic Research-French national research agency), French Embassy in Moscow (Ostrogradski fellowship for young researchers 2020), and French RENATECH network.

## X. APPENDIX

### A. Determination of the NSS absorption from the electron spin noise peak frequencies.

An OMF  $B_1 \cos(2\pi ft)$  along z-axis creates an energy flux towards NSS,  $Q(f, t)$ , corresponding to the energy change per one spin given by

$$Q(f, t) = \frac{\partial E_{\text{NSS}}}{\partial t} = \frac{dB_1}{dt} \sum_i A_i h \gamma_{Ni} I_{zi}, \quad (10)$$

where index  $i$  runs over all isotopes and  $I_{zi}$  is an average projection of the  $i$ -th isotope spin on the OMF direction

$$I_{zi} = \frac{B_1}{h\gamma_{Ni}} \left[ \chi'_f \cos(2\pi ft) - \chi''_f \sin(2\pi ft) \right], \quad (11)$$

$\chi'_f = \chi'_{-f}$  and  $\chi''_f = -\chi''_{-f}$  are real and imaginary parts of the NSS susceptibility, respectively. Therefore, the

averaged over a period energy flux towards NSS  $Q(f)$  is related to its absorption  $\mathcal{A}(f) = f \sum_i A_i \chi''_{fi}$  as

$$Q(f) = \pi B_1^2 \mathcal{A}(f). \quad (12)$$

On the other hand the warm up rate of the NSS in the presence of the OMF reads [1]:

$$\frac{1}{T_w(f)} = \frac{k_B \Theta_N}{C_N} Q(f) = \pi B_1^2 \frac{k_B \Theta_N}{C_N} \mathcal{A}(f). \quad (13)$$

Here  $C_N$  is the heat capacity of the NSS

$$C_N = \frac{I(I+1)}{3} (B^2 + B_H^2) h^2 \sum_i A_i h \gamma_{Ni}^2, \quad (14)$$

$B$  is an arbitrary external static field and  $B_H$  is the heat capacity field introduced in Eq. (1) and rigorously determined as

$$B_H^2 = \frac{3}{I(I+1)} \frac{Sp(\hat{H}_{SS}^2)}{\sum_i A_i h \gamma_{Ni}^2}, \quad (15)$$

where  $\hat{H}_{SS}$  is the total Hamiltonian of all nuclear interactions excluding Zeeman. Thus, NSS absorption at a given spin temperature is proportional to the rate of NSS warm up induced by an OMF.

$T_w(f)$  can be extracted from the experiments described in Section III in a following way. Following Ref. [1], Ch. 5 we can write a detailed balance equation for the inverse nuclear spin temperature  $\beta = 1/k_B \Theta_N$  in the presence of the OMF:

$$\dot{\beta} = -\frac{1}{T_t(f)} (\beta - \beta_t), \quad (16)$$

where

$$\frac{1}{T_t(f)} = \frac{1}{T_w(f)} + \frac{1}{T_1} \quad (17)$$

is the total relaxation rate including OMF-independent relaxation at rate  $T_1$ ,  $\beta_t = \beta_0 (1 + T_w(f)/T_1)^{-1}$  is the steady-state spin temperature and  $\beta_0$  is the steady state temperature for  $B_1 = 0$ .

Nuclear spin temperature is related to the Overhauser field-induced SN frequency component  $F_N$  via Eqs. (2) and (4). Therefore, from Eqs. (16) we obtain

$$\frac{1}{T_t(f)} = \frac{1}{\Delta t_6} \log \left( \frac{F_N(t_7)}{F_N(t_5)} \right), \quad (18)$$

where  $\Delta t_6$  is the duration of the 6-th stage of the RMN experiment, and  $F_N(t_5)$  and  $F_N(t_7)$  are frequencies measured at 5-th and 7-th stages of the RMN experiment, respectively.

Similarly, if  $B_1 = 0$  Eq. (16) becomes

$$\dot{\beta} = -\frac{1}{T_1} (\beta - \beta_0), \quad (19)$$

and

$$\frac{1}{T_1} = \frac{1}{\Delta t_6} \log \left( \frac{F_N^0(t_7)}{F_N^0(t_5)} \right), \quad (20)$$

where  $F_N^0(t_5)$  and  $F_N^0(t_7)$  are frequencies measured at 5-th and 7-th stages of the identical experiment but without OMF ( $B_1 = 0$ ).

$1/T_w(f)$  is recalculated from Eqs. (17), (18) and (20) for each OMF frequency. Since in high-temperature approximation  $\mathcal{A}(f) \propto \beta$ ,  $1/T_w(f)$  does not depend on temperature and thus pertinently characterizes NSS absorption. Therefore,  $1/\pi B_1^2 T_w(f)$  constitutes an NMR spectrum, or a NSS absorption spectrum. Such spectra, normalized to unity and encoded in colors, are shown in Fig. 3 (a, b) for various values of static magnetic field.

### B. Relation between the in-plane stress and energetic parameters of the quadrupole Hamiltonian.

The second rank tensors describing stress  $\sigma_{ij}$  and strain  $\varepsilon_{kl}$  are related by the fourth rank elasticity tensor  $C_{ijkl}$ :

$$\sigma_{ij} = \sum_{k,l} C_{ijkl} \varepsilon_{kl}. \quad (21)$$

In cubic crystals there are only three nonzero components of the elasticity tensor:

$$\begin{aligned} C_{11} &= C_{xxxx} = C_{yyyy} = C_{zzzz}; \\ C_{12} &= C_{xxyy} = C_{yyxx} = C_{xxzz} = C_{zzxx} = C_{yyzz} = C_{zzyy}; \\ C_{44} &= C_{xyxy} = C_{yzzy} = C_{xzxz}. \end{aligned} \quad (22)$$

In a crystalline plate with the normal (z-axis) parallel to the [001] axis, application of the pressure  $p$  in the structure plane at the angle  $\zeta$  to the [100] axis results in appearance of the following components of the stress tensor:

$$\begin{aligned} \sigma_{xx} &= p \cos^2 \zeta \\ \sigma_{yy} &= p \sin^2 \zeta \\ \sigma_{xy} &= \sigma_{yx} = p \cos \zeta \sin \zeta \\ \sigma_{zz} &= \sigma_{zx} = \sigma_{xz} = \sigma_{zy} = \sigma_{yz} = 0 \end{aligned} \quad (23)$$

By expressing components of the stress tensor in Eq. (23) via strain components with Eqs. (21) and (22), one obtains a system of linear equations for strain tensor components that yields the following solutions (see

also problem 3 to 10th section of Chapter 1 in [49]):

$$\begin{aligned}
\varepsilon_{xx} &= p \cdot \frac{(C_{11} + 2C_{12})\cos^2\zeta - C_{12}}{(C_{11} - C_{12})(C_{11} + 2C_{12})} \\
\varepsilon_{yy} &= p \cdot \frac{(C_{11} + 2C_{12})\sin^2\zeta - C_{12}}{(C_{11} - C_{12})(C_{11} + 2C_{12})} \\
\varepsilon_{zz} &= -p \cdot \frac{C_{12}}{(C_{11} - C_{12})(C_{11} + 2C_{12})} \\
\varepsilon_{zx} = \varepsilon_{xz} = \varepsilon_{zy} = \varepsilon_{yz} &= 0 \\
\varepsilon_{xy} = \varepsilon_{yx} &= p \cdot \frac{\cos\zeta \sin\zeta}{C_{44}}. \tag{24}
\end{aligned}$$

In the general case, the stress can be applied along two orthogonal axes in the plane. If now the angle  $\zeta$  defines the direction of one of the two principal axes of the stress tensor in the plane, principal values of this tensor being  $p_1$  and  $p_2$ , then due to linearity of Eqs. (24) we get:

$$\begin{aligned}
\varepsilon_{xx} &= \frac{(C_{11} + 2C_{12})(p_1 \cos^2\zeta + p_2 \sin^2\zeta) - C_{12}(p_1 + p_2)}{(C_{11} - C_{12})(C_{11} + 2C_{12})} \\
\varepsilon_{yy} &= \frac{(C_{11} + 2C_{12})(p_1 \sin^2\zeta + p_2 \cos^2\zeta) - C_{12}(p_1 + p_2)}{(C_{11} - C_{12})(C_{11} + 2C_{12})} \\
\varepsilon_{zz} &= -\frac{C_{12}(p_1 + p_2)}{(C_{11} - C_{12})(C_{11} + 2C_{12})} \\
\varepsilon_{zx} = \varepsilon_{xz} = \varepsilon_{zy} = \varepsilon_{yz} &= 0 \\
\varepsilon_{xy} = \varepsilon_{yx} &= (p_1 - p_2) \cdot \frac{\cos\zeta \sin\zeta}{C_{44}}. \tag{25}
\end{aligned}$$

Thus, with the knowledge of the strain components one can find the energetic parameters of the quadrupole Hamiltonian [11]:

$$\begin{aligned}
E_{QZ} &= \frac{3eQS_{11}}{2I(2I-1)} \left( \varepsilon_{zz} - \frac{\varepsilon_{xx} + \varepsilon_{yy}}{3} \right) \\
E_{QR} &= \frac{3\sqrt{3}eQS_{11}}{4I(2I-1)} (\varepsilon_{xx} - \varepsilon_{yy}) \\
E_{QI} &= \frac{\sqrt{3}eQS_{44}}{2I(2I-1)} (\varepsilon_{xy} + \varepsilon_{yx}) \tag{26}
\end{aligned}$$

which amount to (cf Eqs. (3) and (7)-(9)):

$$\begin{aligned}
E_{QZ} &= \frac{3eQS_{11}}{4I(2I-1)} \frac{1}{C_{11} - C_{12}} (p_1 + p_2) \\
E_{QR} &= \frac{3\sqrt{3}eQS_{11}}{4I(2I-1)} \frac{\cos(2\zeta)}{C_{11} - C_{12}} (p_1 - p_2) \\
E_{QI} &= \frac{\sqrt{3}eQS_{44}}{2I(2I-1)} \frac{\sin(2\zeta)}{C_{44}} (p_1 - p_2) \tag{27}
\end{aligned}$$

- 
- [1] F. Meier and B. P. Zakharchenya, eds., *Optical Orientation* (North Holland, Amsterdam, 1984).
- [2] S. Foletti, H. Bluhm, D. Mahalu, V. Umansky, and A. Yacoby, *Nature Physics* **5**, 903 (2009).
- [3] H. Bluhm, S. Foletti, I. Neder, M. Rudner, D. Mahalu, V. Umansky, and A. Yacoby, *Nature Physics* **7**, 109 (2010).
- [4] E. A. Chekhovich, M. N. Makhonin, A. I. Tartakovskii, A. Yacoby, H. Bluhm, K. C. Nowack, and L. M. K. Vandersypen, *Nature Publishing Group* **12**, 494 (2013).
- [5] B. Urbaszek, X. Marie, T. Amand, O. Krebs, P. Voisin, P. Maletinsky, A. Högele, and A. Imamoglu, *Reviews of Modern Physics* **85**, 79 (2013).
- [6] R. Stockill, C. Le Gall, C. Matthiesen, L. Huthmacher, E. Clarke, M. Hugues, and M. Atatüre, *Nature Communications* **7**, 12745 (2016).
- [7] D. A. Gangloff, G. Éthier-Majcher, C. Lang, E. V. Denning, J. H. Bodey, D. M. Jackson, E. Clarke, M. Hugues, C. Le Gall, and M. Atatüre, *Science* **364**, 62 (2019).
- [8] E. V. Denning, D. A. Gangloff, M. Atatüre, J. Mørk, and C. Le Gall, *Physical Review Letters* **123**, 140502 (2019).
- [9] E. A. Chekhovich, S. F. C. da Silva, and A. Rastelli, *Nature Nanotechnology* **15**, 999 (2020).
- [10] D. A. Gangloff, L. Zaporski, J. H. Bodey, C. Bachorz, D. M. Jackson, G. Éthier-Majcher, C. Lang, E. Clarke, M. Hugues, C. Le Gall, and M. Atatüre, *Nature Physics* (2021), 10.1103/PhysRevB.10.4244.
- [11] A. Abragam, *The principles of nuclear magnetism* (Clarendon Press, 1961).
- [12] R. I. Dzhiyev and V. L. Korenev, *Physical Review Letters* **99**, 037401 (2007).
- [13] P. Maletinsky, M. Kroner, and A. Imamoglu, *Nat. Phys.* **5**, 407 (2009).
- [14] E. A. Chekhovich, K. V. Kavokin, J. Puebla, A. B. Krysa, M. Hopkinson, A. D. Andreev, A. M. Sanchez, R. Beanland, M. S. Skolnick, and A. I. Tartakovskii, *Nat. Nanotech.* **7**, 646 (2012).
- [15] R. K. Sundfors, *Physical Review B* **10**, 4244 (1974).
- [16] E. A. Chekhovich, I. M. Griffiths, M. S. Skolnick, H. Huang, S. F. C. da Silva, X. Yuan, and A. Rastelli, *Phys. Rev. B* **97**, 235311 (2018).
- [17] I. M. Griffiths, H. Huang, A. Rastelli, M. S. Skolnick, and E. A. Chekhovich, *Phys. Rev. B* **99**, 125304 (2019).
- [18] V. M. Litvyak, R. V. Cherbunin, V. K. Kalevich, A. I. Lihachev, A. V. Nashchekin, M. Vladimirova, and K. V. Kavokin, "Warm-up spectroscopy of quadrupole-split nuclear spins in n-gaas epitaxial layers," (2021), arXiv:2105.03972 [cond-mat.mes-hall].
- [19] I. I. Ryzhov, S. V. Poltavtsev, K. V. Kavokin, M. M. Glazov, G. G. Kozlov, M. Vladimirova, D. Scalbert, S. Cronenberger, A. V. Kavokin, A. Lemaître, J. Bloch, and V. S.

- Zapasskii, Applied Physics Letters **106**, 242405 (2015).
- [20] V. K. Kalevich, K. V. Kavokin, I. Merkulov, and M. Vladimirova, in *Spin Physics in Semiconductors*, edited by M. I. Dyakonov (Springer International Publishing, Cham, 2017) pp. 387–430.
- [21] M. M. Glazov, Physical Review B **91**, 195301 (2015).
- [22] M. M. Glazov, *Electron & Nuclear Spin Dynamics in Semiconductor Nanostructures* (OUP Oxford, 2018).
- [23] E. Alexandrov and V. P. Zapasskii, ZETP **81**, 132 (1981).
- [24] M. Römer, J. Hübner, and M. Oestreich, Review of Scientific Instruments **78**, 103903 (2007).
- [25] S. Cronenberger and D. Scalbert, Review of Scientific Instruments **87**, 093111 (2016).
- [26] P. Sterin, J. Wiegand, J. Hübner, and M. Oestreich, Phys. Rev. Applied **9**, 034003 (2018).
- [27] M. Y. Petrov, A. N. Kamenskii, V. S. Zapasskii, M. Bayer, and A. Greilich, Phys. Rev. B **97**, 125202 (2018).
- [28] M. Vladimirova, S. Cronenberger, D. Scalbert, M. Kotur, R. I. Dzhioev, I. I. Ryzhov, G. G. Kozlov, V. S. Zapasskii, A. Lemaître, and K. V. Kavokin, Phys. Rev. B **95**, 125312 (2017).
- [29] M. Vladimirova, S. Cronenberger, D. Scalbert, I. I. Ryzhov, V. S. Zapasskii, G. G. Kozlov, A. Lemaître, and K. V. Kavokin, Phys. Rev. B **97**, 041301 (2018).
- [30] D. Paget, G. Lampel, B. Sapoval, and V. I. Safarov, Phys. Rev. B **15**, 5780 (1977).
- [31] This field was sometimes called local field despite the quadrupole contribution [? ], but for the sake of clarity we prefer using the term heat capacity field.
- [32] The intended direction of the OMF was along z-axis. Its in-plane component is presumably due to eddy currents in the copper-based sample holder.
- [33] J. Hübner, F. Berski, R. Dahbashi, and M. Oestreich, physica status solidi (b) **251**, 1824 (2014).
- [34] The dipole-dipole interaction which is known to broaden the NMR transitions, but does not lead to any shifts of their energies, is not included here[11].
- [35] A. Abragam and W. G. Proctor, Phys. Rev. **109**, 1441 (1958).
- [36] V. K. Kalevich, V. D. Kulkov, and V. G. Fleisher, JETP Lett. **35**, 20 (1982).
- [37] M. I. Dyakonov, ed., *Spin Physics in Semiconductors*, Vol. 157 (Springer International Publishing, 2017).
- [38] P. Pyykkö, Molecular Physics **106**, 1965 (2008).
- [39] Y. A. Burenkov, Y. M. Burdukov, S. Y. Davidov, and S. P. Nikanorov, Sov. Phys. Solid State **15**, 1175 (1973).
- [40] M. Yamada, Applied Physics Letters **47**, 365 (1998).
- [41] M. Eickhoff, B. Lenzmann, D. Suter, S. E. Hayes, and A. D. Wieck, Phys. Rev. B **67**, 085308 (2003).
- [42] A. Brunetti, M. Vladimirova, S. Cronenberger, D. Scalbert, M. Nawrocki, and J. Bloch, Superlattices and Microstructures **41**, 429 (2007).
- [43] M. Abbarchi, C. Diederichs, L. Largeau, V. Ardizzone, O. Mauguin, T. Lecomte, A. Lemaître, J. Bloch, P. Roussignol, and J. Tignon, Physical Review B **85**, 045316 (2012).
- [44] L. F. Lastras-Martínez, E. Cerda-Méndez, N. Ulloa-Castillo, R. Herrera-Jasso, L. E. Rodríguez-Tapia, O. Ruiz-Cigarrillo, R. Castro-García, K. Biermann, and P. V. Santos, Physical Review B **96**, 4244 (2017).
- [45] M. Kotur, R. I. Dzhioev, M. Vladimirova, B. Jouault, V. L. Korenev, and K. V. Kavokin, Phys. Rev. B **94**, 081201 (2016).
- [46] The same formula wher used in Ref. 18.
- [47] Using the values of Sundfors [15] would give approximately a factor of 1.4 smaller values of  $p_1$  and  $p_2$ .
- [48] J. W. Blanchard, D. Budker, and A. Trabesinger, Journal of Magnetic Resonance **323**, 106886 (2021).
- [49] L. D. Landau, L. P. Pitaevskii, A. M. Kosevich, and E. M. Lifshitz, *Theory of Elasticity Volume 7* (Elsevier Science, 2012).